


Article

A Novel SWB Antenna with Triple Band-Notches Based on Elliptical Slot and Rectangular Split Ring Resonators

Xiaobo Zhang ¹, Saeed Ur Rahman ^{2,*}, Qunsheng Cao ², Ignacio Gil ³ 
and Muhammad Irshad Khan ⁴

¹ School of Automation, Guangdong University of Technology, Guangzhou 510006, China; zxb_leng@gdut.edu.cn

² College of Electronic and Information Engineering, Nanjing University of Aeronautics and Astronautics (NUAA), Nanjing 210016, China; qunsheng@nuaa.edu.cn

³ Department of Electronic Engineering, Universitat Politècnica de Catalunya, 08222 Terrassa, Spain; Ignasi.gil@upc.edu

⁴ Department of Electrical Engineering, University of Engineering and Technology, Peshawar 54890, Kohat Campus, Pakistan; irshadnawab@outlook.com

* Correspondence: saeed@nuaa.edu.cn; Tel.: +86-19850860016

Received: 18 December 2018; Accepted: 2 February 2019; Published: 10 February 2019



Abstract: In this paper, a wideband antenna was designed for super-wideband (SWB) applications. The proposed antenna was fed with a rectangular tapered microstrip feed line, which operated over a SWB frequency range (1.42 GHz to 50 GHz). The antenna was implemented at a compact size with electrical dimensions of $0.16 \lambda \times 0.27 \lambda \times 0.0047 \lambda \text{ mm}^3$, where λ was with respect to the lowest resonance frequency. The proposed antenna prototype was fabricated on a F4B substrate, which had a permittivity of 2.65 and 1 mm thickness. The SWB antenna exhibited an impedance bandwidth of 189% and a bandwidth ratio of 35.2:1. Additionally, the proposed antenna design exhibited three band notch characteristics that were necessary to eradicate interference from WLAN, WiMAX, and X bands in the SWB range. One notch was achieved by etching an elliptical split ring resonator (ESRR) in the radiator and the other two notches were achieved by placing rectangular split ring resonators close to the signal line. The first notch was tuned by incorporating a varactor diode into the ESRR. The prototype was experimentally validated with, with notch and without notch characteristics for SWB applications. The experimental results showed good agreement with simulated results.

Keywords: split ring resonator; super wideband; tri-notch

1. Introduction

In advanced wireless communication, the demand for super-wideband (SWB) antennas is on the rise. SWB antennas cover both long-range and short-range communication that includes the ultra-wideband (UWB) range. For such applications, the monopole antenna is a good candidate owing to its low cost and ease of fabrication, but the comparatively large size of such an antenna is a major drawback. The fractional bandwidth of SWB antennas should be at least 10:1, with a maximum percent bandwidth and bandwidth dimension ratio (BDR). The BDR tells us about the compactness and wideband characteristics of the antenna.

In the literature, many antennas have been designed for SWB applications [1–10]. In [8], a SWB antenna was designed with a coaxial feed. The shape of the antenna was fractal, providing band operation from 10 GHz to 50 GHz with low BDR and at a lower resonant frequency of 10 GHz. In [9], a compact SWB monopole antenna was designed with dimensions of $0.17 \lambda \times 0.37 \lambda \times 1.6 \text{ mm}^3$.

The proposed antenna could operate from 1.44 GHz to 18 GHz, having a bandwidth (BW) ratio of 13.06:1. In the literature, the major issues were large, including lowest resonance frequency and low BDR. The main goals in the design of SWB antennas are to achieve a compact size, maximum bandwidth, and a high BDR.

In UWB and SWB systems, there is a coexistence of the narrow bands such as WLAN, WiMAX and X band. A stopband characteristic can be added to SWB antennas. The purpose of the stop band characteristics is to reduce the radiation of the coexisted bands in the UWB or in the SWB range. Many antennas have been designed for UWB application with notch characteristics. UWB antennas with single notch [11,12] dual notch [13], tri-notch [14–18], and quad-notch [19,20] and [21,22] quintuple notched antennas have been designed. The single, dual, tri- and multiple notch characteristics have been achieved in the UWB frequency range (3.1 GHz–10.6 GHz). In the reported literature, the designed notched antennas are unable to operate within SWB frequency range. Few antennas have been designed for SWB application with notch characteristics. In [23,24], SWB antennas were designed with single notch characteristic and also in [25,26], SWB antennas were designed with dual notch characteristics. In [25], the notch characteristics were achieved by inserting slots. A tri-notch characteristic SWB antenna was designed in [6], with the BW ratio of the designed antenna being 34:1. The notch characteristics in [6], were achieved by inserting the arc and U-shape slots in the radiator and ground, respectively. The size of the proposed design was very large, that is, measuring approximately $150 \times 150 \text{ mm}^2$. In the literature, mostly monopole antennas have been designed for SWB application without notch characteristics. The important issues in the designing of SWB antennas are miniaturization, and also to eradicate the inference of narrow bands such as WLAN, WiMAX, and X bands within SWB frequency range.

In this paper, a SWB antenna was designed with and without notch characteristics. The proposed SWB antenna was based on a trapezoid shape radiator and semicircular ground. The bandwidth performance of a trapezoid shape radiator, semicircular ground, and rectangular tapered feed line showed better bandwidth performance with the lowest resonance frequency of 1.42 GHz. In addition, three notch characteristics were achieved in the SWB range. Among these notches, two notches were achieved by incorporating a rectangular split ring resonator (RSRR) near the feed line and the third notch was achieved by incorporating an elliptical split ring resonator (ESRR) in the radiator. Moreover, a varactor diode was incorporated into the isolated area in the elliptical slot to make the center notch frequency tuned from 1.9 GHz to 2.5 GHz.

2. The Design of the SWB Antenna

The design procedure of the SWB antenna is shown in Figure 1a–d. In Figure 1a, a monopole antenna was designed with rectangular shaped, radiator, ground, and feed line. The monopole antenna with a rectangular shape showed mismatching for lower frequencies and worse matching for higher frequencies, as shown in Figure 2. Bandwidth performance of wideband monopole antennas are dependent on the longest current path followed, so the proposed rectangular radiator was a modified trapezoid shape as shown in Figure 1b, and also the ground was modified to a semicircular shape as shown in Figure 1c. From Figure 2, it can be observed that the bandwidth performance was improving with modifying the radiator and ground. To achieve optimal matching, the feed line was modified to be rectangular to the tapered line [27]. The width of the rectangular tapered feed line linearly decreased towards the radiator as shown in Figure 1d, and that covered the maximum range of resonance frequencies. The length and width of the rectangular feed line was calculated using standard equations as given in [28]. The substrate of the proposed design was F4B with permittivity of 2.65 and a thickness of 1 mm where the final schematic is shown in Figure 3 and its dimensions are listed in Table 1.

Table 1. The dimension of the proposed tri-notch characteristics SWB antenna.

Dimension	Value (mm)	Dimension	Value (mm)
W_s	34.0	W_{c1}	2.5
W_1	5.0	L_{c1}	5.0
W_2	34.0	W_{c2}	4.0
W_{s1}	0.5	L_{c2}	8.0
W_{s2}	0.4	W_{50}	2.5
W_{g1}	0.6	e_x	7.0
W_{g2}	0.6	e_y	4.5
L_s	57		

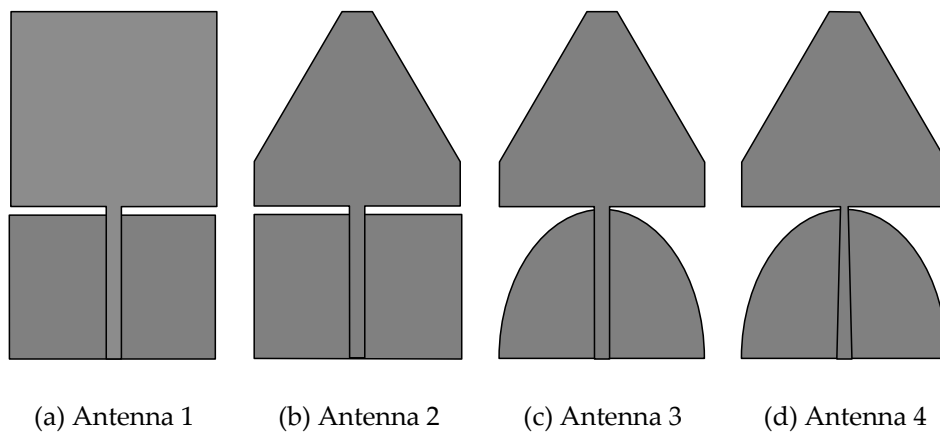


Figure 1. The geometry of a super-wideband (SWB) antenna with: (a) Rectangular ground and radiator; (b) rectangular ground and trapezoid radiator; (c) trapezoid radiator and semicircular ground; (d) semicircular ground, trapezoid radiator, and rectangular tapered feed.

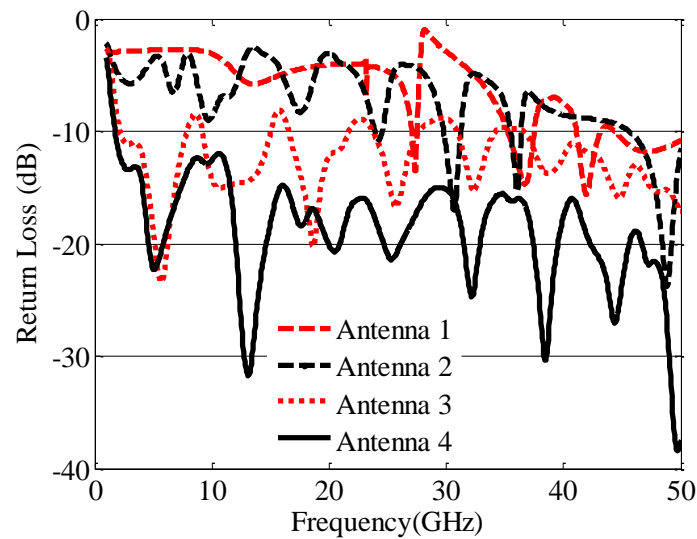


Figure 2. The simulated return loss for designed SWB antennas in Figure 1.

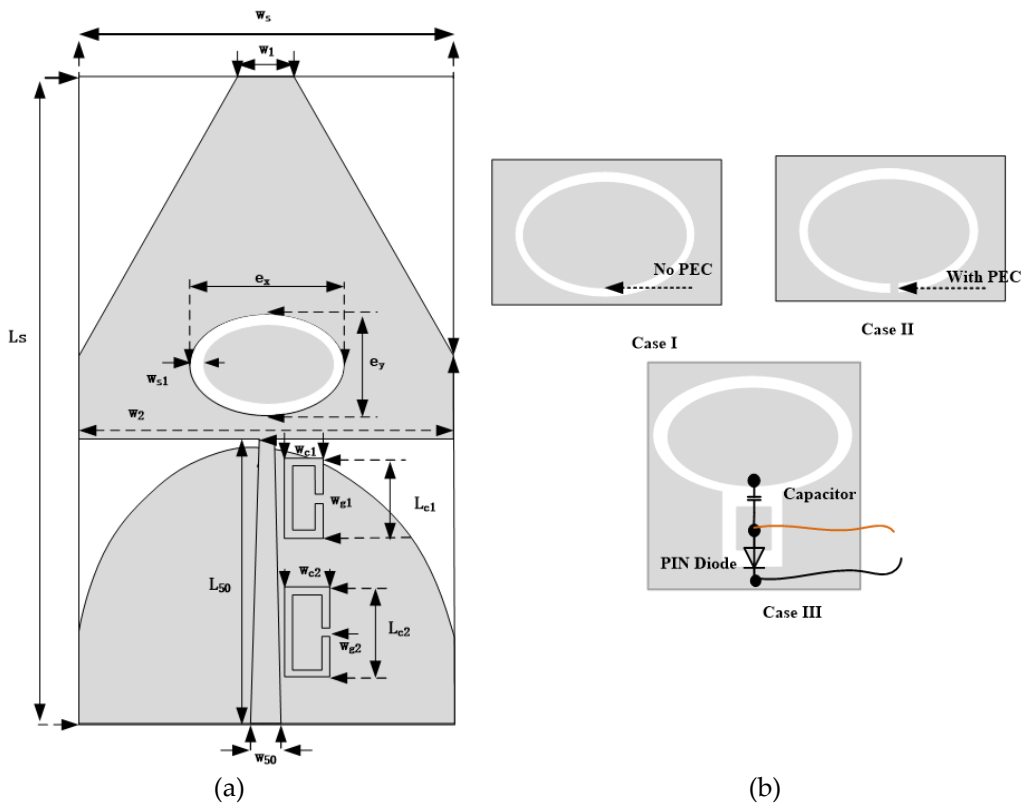


Figure 3. The schematic diagram of: (a) notch characteristics of a SWB antenna; (b) different cases of elliptical slots.

The simulations were carried out using commercial software computer simulation technology (CST) version 2016. The simulated results showed maximum matching from 1.42 GHz to 50 GHz without incorporating any notch. The fabricated prototype of the proposed SWB antenna is shown in Figure 4. The fabricated prototype was verified using an Agilent network analyzer. For the S11 measurement, Keysight’s Network Analyzer model# N5245A was used. Port 1 was calibrated using a mechanical toolkit 85056A Calibration Kit system. Then, the antenna was connected to measure its accurate response. The simulated and measured return loss is illustrated in Figure 5. As can be seen, the measured results were in good agreement with the simulated results. From the measured result, the impedance matching becomes worse around about 35 GHz to 40 GHz. This is because of the measuring device, as the network analyzer showed noise at those frequencies, or it may be due to the quality of the SMA connectors and scattering measurement environment.

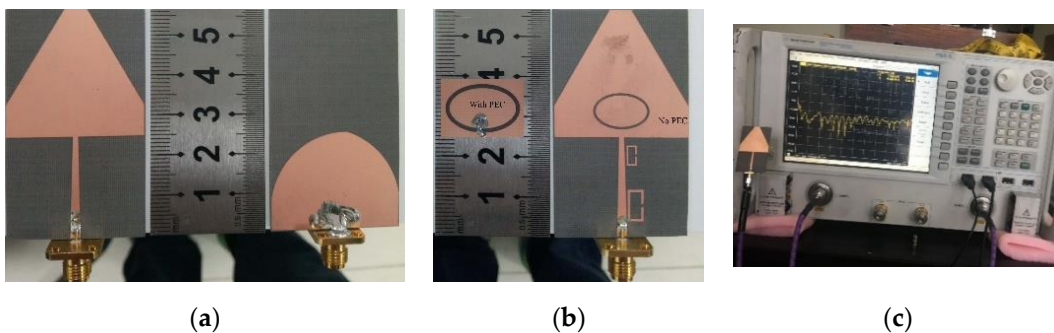


Figure 4. The fabricated prototype: (a) Top side and back side of without notch; (b) top side of band notch of SWB antenna; and (c) a photograph of measuring device.

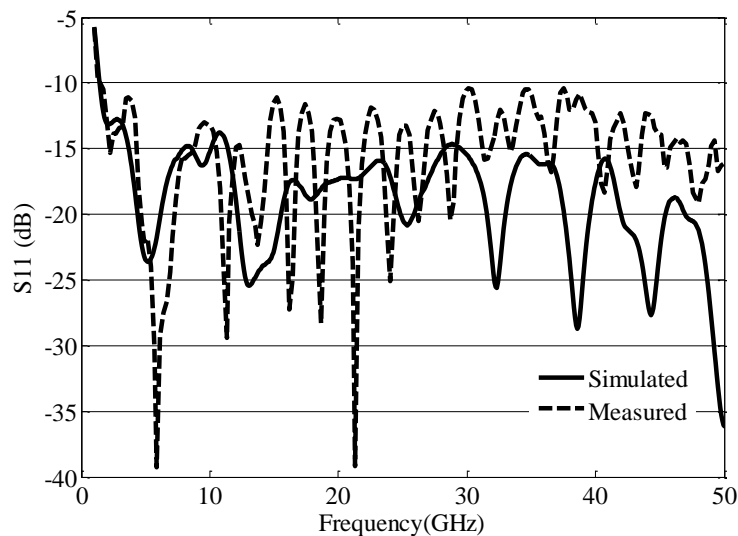


Figure 5. The simulated and measured return loss.

The lower resonance frequency of the simulated and measured results was around 1.42 GHz, while the higher resonance frequency was above 50 GHz. Where the peak gain plot is also depicted in Figure 6. However, due to available resources, we have measured the matching performance of SWB antennas up to 50 GHz. Figure 6 shows the simulated and measured peak gain of the SWB antenna. The SWB antenna showed an acceptable gain in the frequency range from 1.42 GHz to 50 GHz. However, the peak gain of the SWB was increased at higher frequencies, because the dimension of the radiator was larger than its corresponding wavelength.

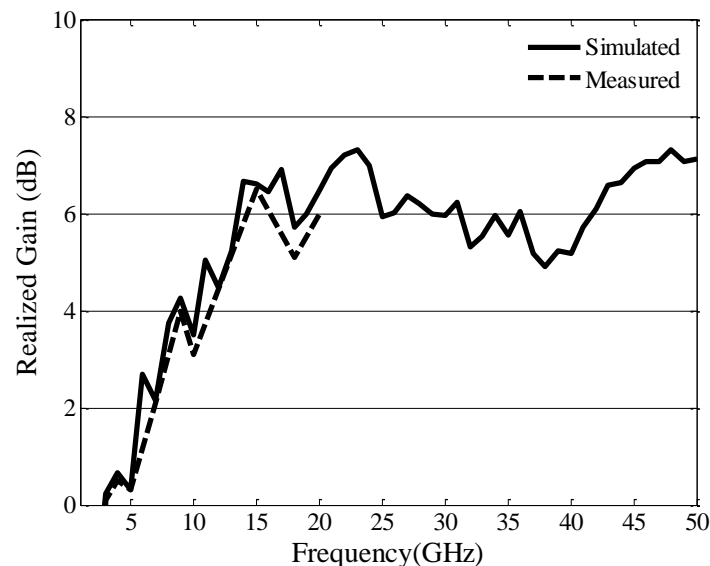


Figure 6. The simulated and measured peak gain.

3. Simulation and Measurements

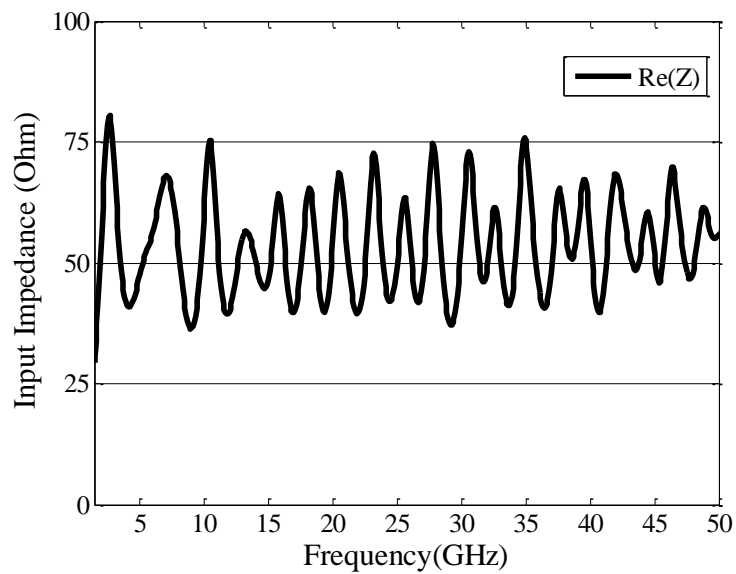
3.1. The Proposed SWB Antenna

The base antenna was composed of a printed monopole and trapezoid shape radiator shown in Figure 3a. The electrical dimensions of the proposed SWB monopole antenna were $0.16\lambda \times 0.27\lambda \times 1\text{mm}^3$, where λ was with respect to the lowest resonance frequency, and the electrical dimensions were calculated using Equation (1). The matching performance of the SWB antenna is also shown in Figure 7a–d, in the form of input characteristic impedance. In Figure 7a,b, the real and imaginary parts

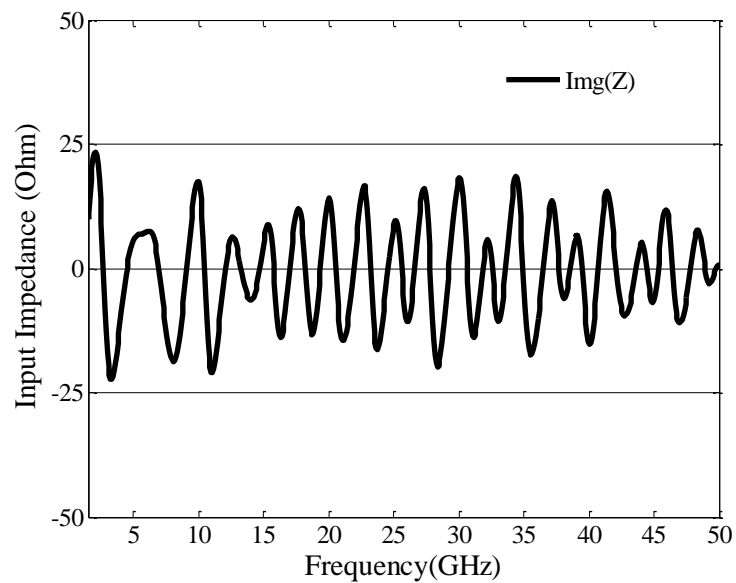
of the simulated input impedance were about 50Ω and 0Ω , respectively, over the operating frequency range. In Figure 7c, the magnitude of the impedance was around 50Ω . The variations in the real and imaginary values of the characteristic's impedance provided approximated characteristic impedance of the SMA connector, which showed a good matching between the input and characteristic impedance of the SMA. The Smith chart has been plotted in Figure 7d, with the minimum impedance being about 20 ohm and the maximum being around about 50 ohms . Overall, the impedance was varying around 50 ohms .

$$\text{Elec. dim.} = \frac{\text{physical dim.}}{\lambda} \quad (1)$$

where $\lambda = c/f$.



(a)



(b)

Figure 7. Cont.

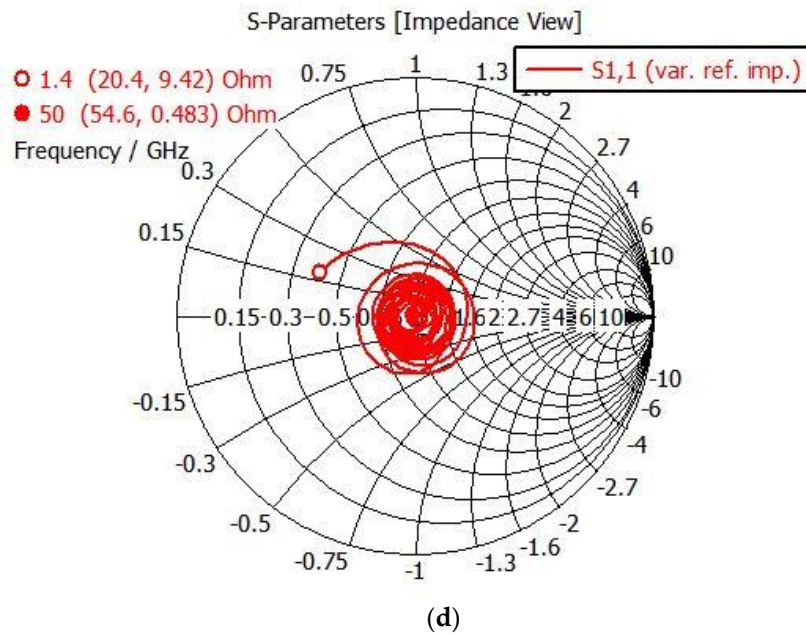
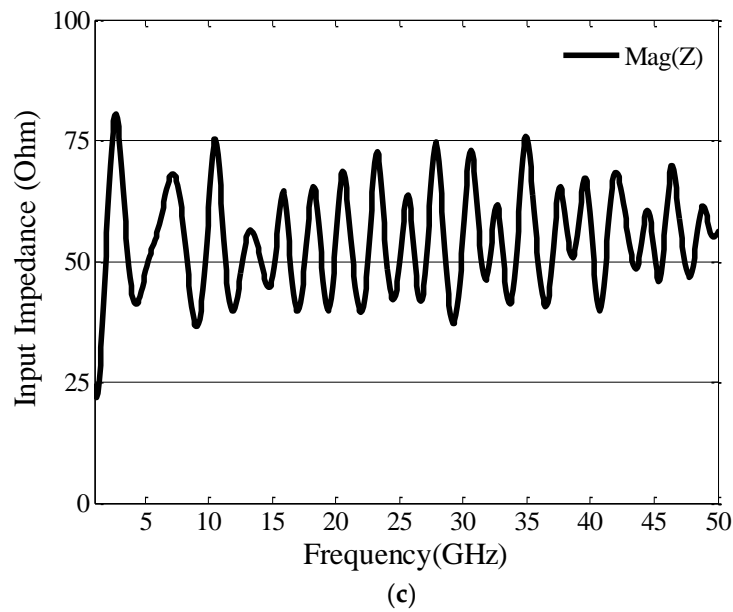


Figure 7. The input impedance of a designed SWB antenna: (a) Real; (b) imaginary part; (c) magnitude; (d) Smith chart.

The index term BDR signifies how much operating bandwidth in percent could be provided per unit electrical area. It also shows the structure’s compactness and the range of bandwidth covered by the proposed structure. The BDR can be mathematically expressed as:

$$BDR = \frac{BW\%}{\lambda_{length} \times \lambda_{width}} \tag{2}$$

The λ represents the wavelength corresponding to the lowest cut-off frequency of the operating bandwidth. A large value of BDR was desirable to validate the effectiveness of the proposed structure over other existing designed structures. The comparative results of the proposed antenna design and currently available antenna designs are presented in Table 2. From Table 2, it is observed that the

proposed design exhibited better performance in terms of one of the calculated parameters such as %BW, BDR, and BW ratio, and the lowest resonance frequency.

Table 2. Comparison with previously reported SWB antennas.

Ref.	Dimension	BW:1	%BW	BDR	Freq: Range (GHz)	Notch Function
[1]	$0.37\lambda \times 0.34\lambda$	34.88	189.00	1502	0.86–30	No
[2]	$0.36\lambda \times 0.24\lambda$	22.10	183.00	2118	0.79–17.4	No
[3]	$0.33\lambda \times 0.25\lambda$	32.00	187.00	2286	2.5–80	No
[7]	$0.45\lambda \times 0.45\lambda$	19.40	180.00	889	1.00–19.4	No
[8]	$2.0\lambda \times 2.0\lambda$	5.00	133.00	33	10.00–50.00	No
[9]	$0.37\lambda \times 0.17\lambda$	13.06	172.00	2763	1.44–18.8	No
[10]	$0.38\lambda \times 0.36\lambda$	40.00	190.00	1389	0.72–18	No
[29]	$0.30\lambda \times 0.23\lambda$	9.80	163.00	2362.	2.26–22.18	No
[30]	$0.55\lambda \times 0.38\lambda$	11.60	168.00	803	3.00–35	No
[31]	$0.31\lambda \times 0.46\lambda$	10.16	164.10	1102	3.15–32	No
[32]	$0.33\lambda \times 0.23\lambda$	20.40	181.30	2461.5	2.18–44.5	No
[33]	$0.27\lambda \times 0.18\lambda$	11.60	168.25	3462	2.5–29	No
[34]	$0.32\lambda \times 0.34\lambda$	11.00	166.67	1531.89	3.4–37.4	No
[35]	$0.26\lambda \times 0.28\lambda$	31.10	187.00	2569	1.06–32.7	No
[36]	$0.31\lambda \times .27\lambda$	10.67	166.00	1948	2.7–28.8	No
[37]	$0.33\lambda \times .20\lambda$	11.60	168.00	2386	3.0–35	No
[38]	$0.41\lambda \times 0.29\lambda$	10.11	166.66	1347.24	3.5–31	No
Proposed	$0.16\lambda \times 0.27\lambda$	35.21	189.00	4375	1.42–50	Yes

3.2. The RSRR

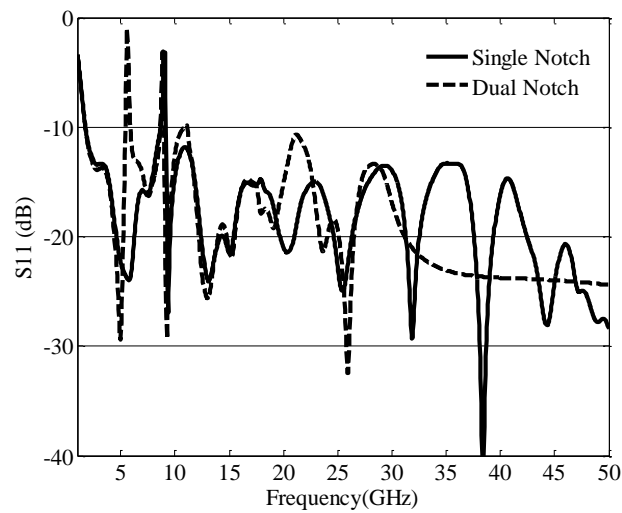
In this section, the rectangular ring resonator was designed and placed near the feed line, about 1.45 mm from the feed line center in a horizontal x-direction. High magnetic coupling was produced between the resonator and a signal line, which reduced the radiation energy in the desired band i.e., WLAN, WiMAX etc. Two RSRRs had been designed for achieving two notch resonance frequencies. The dimensions of RSRR could be calculated by using the following equations [39].

$$S_1 = 2(L_{cn} + W_{cn} - 2w_{s2}) = \frac{\lambda_g}{2} = \frac{c}{2f_n \sqrt{\epsilon_{eff}}} \quad (3)$$

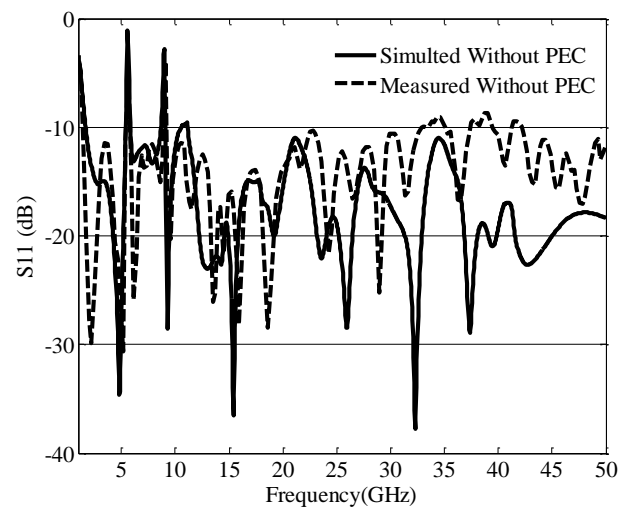
$$\epsilon_{eff} = \frac{\epsilon_r + 1}{2} + \frac{\epsilon_r - 1}{2} \left(1 + \frac{12h}{W_{50}}\right)^{-0.5} \quad (4)$$

where S_1 is the inner perimeter of the single RSRR that is a function of length (L_{cn}), width (W_{cn}), and strip width (w_{s2}), where $n = 1, 2$. The effective permittivity (ϵ_{eff}) is given in Reference [28]. At the notch resonance frequency, the perimeter (S_1) should be half of the guided wavelength (λ_g). In order to achieve the notch resonance frequency at 8.8 GHz, a single RSRR having width (W_{c1}) and length (L_{c1}) was placed close to the signal line.

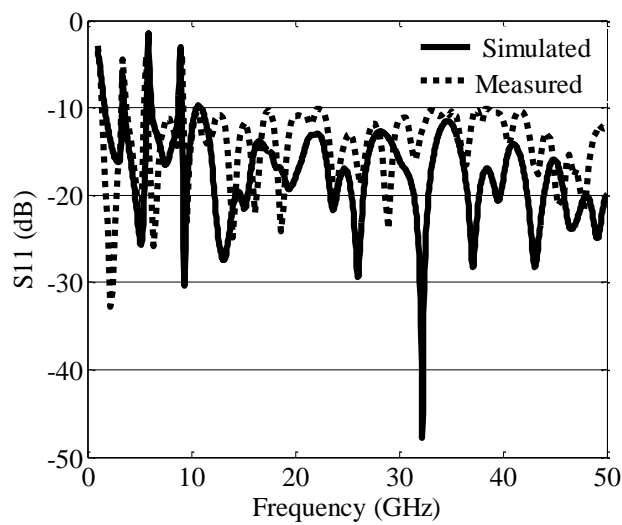
Similarly, for the second notch resonant frequency at 5.6 GHz, another RSRR having width (W_{c2}) and length (L_{c2}) was placed close to the signal line. The dimensions of the resonator controlled the resonance notch frequency. By changing the dimensions of the RSRR, the resonance notch frequency could be shifted easily. In the SWB frequency range, single notch resonance and dual notch resonance frequencies have been shown in Figure 8a. From Figure 8a, it can be noted that by loading one RSRR, the single notch was achieved at 9 GHz. In the same way, by loading two RSRRs, two notch frequencies at 8.8 GHz and 5.6 GHz were achieved.



(a)



(b)



(c)

Figure 8. The simulated return loss for: (a) Loading single and dual rectangular split ring resonators (RSRRs); (b) simulated and measured return loss for the case I of Figure 3; (c) simulated and measured return loss for case II of Figure 3.

3.3. ESRR

For achieving the third notch, an ESRR was etched out from the radiating patch. The major axis of the ESRR was e_x , the minor axis was e_y , and width was w_{s1} . To achieve the notch at a certain frequency, the following equations were employed to compute the dimensions of the ESRR [39].

$$S_2 = K_e \pi (0.5e_y - w_{s1}) = \frac{\lambda_g}{2} = \frac{c}{2f_n \sqrt{\epsilon_{eff}}} \quad (5)$$

$$K_e = 3(1+k) - \sqrt{(3+k)(1+3k)} \quad (6)$$

Here, S_2 was the inner circumference of the elliptical slot of the split ring. The circumference should be half the guided wavelength λ_g at the desired notch frequency. The factor K_e was used for the calculation of the circumference of the ellipse with ellipticity ($k = e_x/e_y$). The major and minor axes were adjusted according to the above equations for 3.6 GHz. The major axis (e_x) was taken about 12.4 mm, the minor axis (e_y) about 7.4 mm and the width (w_{s1}) was about 0.5 mm.

The single and dual notch characteristics were achieved by loading single and dual RSRRs near the feed line. The return loss for single and dual notch characteristics are shown in Figure 8a. Case I for the elliptical slot is shown in Figure 3. For case I, a PEC patch with a width of 0.3 mm was placed in the slot, with a width (w_{s1}) that connected the inner elliptical patch with the radiator for achieving the third notch at 3.6 GHz. In case II, the rejection at 3.6 GHz was eliminated by removing the PEC, and the resulting structure exhibited dual notch characteristics. Therefore, the proposed SWB antenna could be reconfigured if a PIN diode was incorporated into the elliptical slot. The simulated and measured return loss for case I and case II are shown in Figure 8b,c, respectively. The measured results showed a good agreement with simulated results for both the cases. The comparative results of the notched characteristics antenna are shown in Table 2. The major issue in the previously designed antennas was a large size, and to eradicate the interfered narrow band. In the previous research work, most antennas had no function to eradicate single, dual, and tri-band. The bandwidth performance was also important for SWB notch characteristic antennas.

Additionally, simulations were carried out to tune the third notched band at 3.6 GHz. Lumped capacitor and varactor diode were incorporated into the isolated area of an elliptical slot, where the varactor diode acted as a variable capacitor as shown in case III of Figure 3. The embedded varactor diode tuned a third notch frequency at 3.6 GHz, and it was controlled by changing the capacitance. The proposed varactor diode was SMV2201 and was embedded in an isolated area. With increasing the capacitance C of the varactor diode from 0.23 pF to 2.1 pF, the center notch frequency changed from 1.9 GHz to 2.52 GHz. The simulated return loss with the tuned band is shown in Figure 9. In the isolated area, a capacitor with a value of 1pF was employed to block the dc voltage from the external dc source. Moreover, simulations were carried out to see the effect of the SRR. The dimensions of the resonators have been varied. It is observed from Figure 10 that when the length of the RSRR was increased, then according to Equation (2), the notch band was shifted to lower frequency resonance. This was similar, for the ESRR.

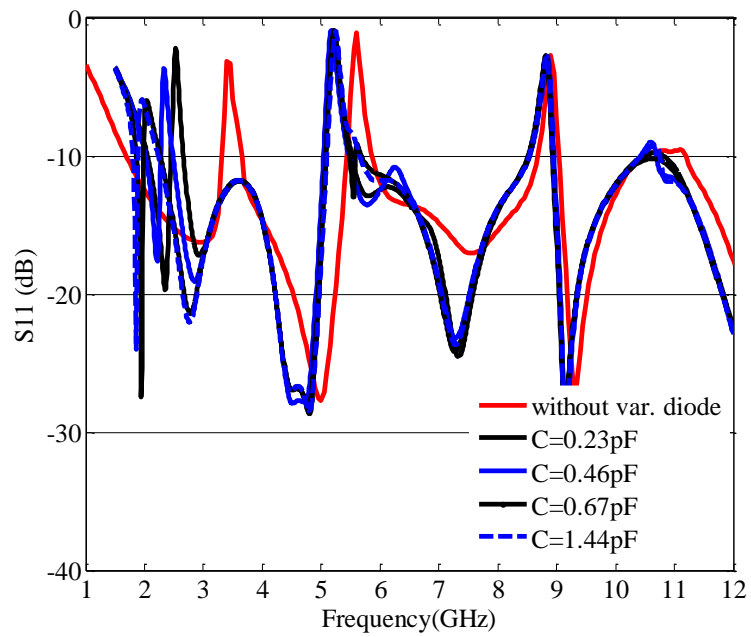


Figure 9. Simulated return loss with tunable notch frequency for case III in Figure 3.

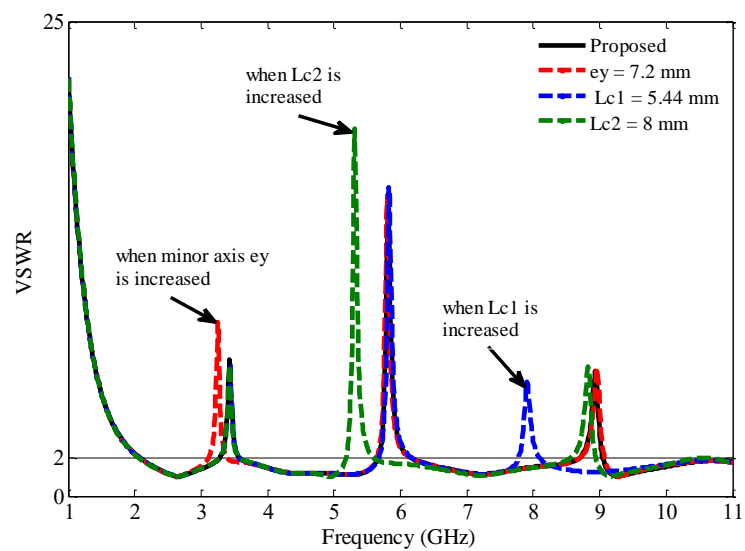


Figure 10. Parametric study of the resonator.

3.4. The Gain, Current Distribution, and Pattern

The simulated current distribution of band notched SWB antenna is shown in Figure 11a–c for each resonance mode. For the optimal design, the simulated current distribution at 3.4 GHz is shown in Figure 11a. The current was mainly concentrated on the left and right side of the PEC, where the PEC was the connecting patch between the elliptical patch and radiator, as shown in case I of Figure 3. The current flowed in the opposite direction at the edge of the radiator and of the elliptical slot. Meanwhile, the current distribution did not exist around the other loaded RSRR. This implies that the ESRR was critical for the generation of a stop band at 3.4 GHz. Similarly, with two loaded resonators near the signal line influence, the notch bands at 5.6 GHz and 9 GHz are shown in Figure 11b,c, respectively.

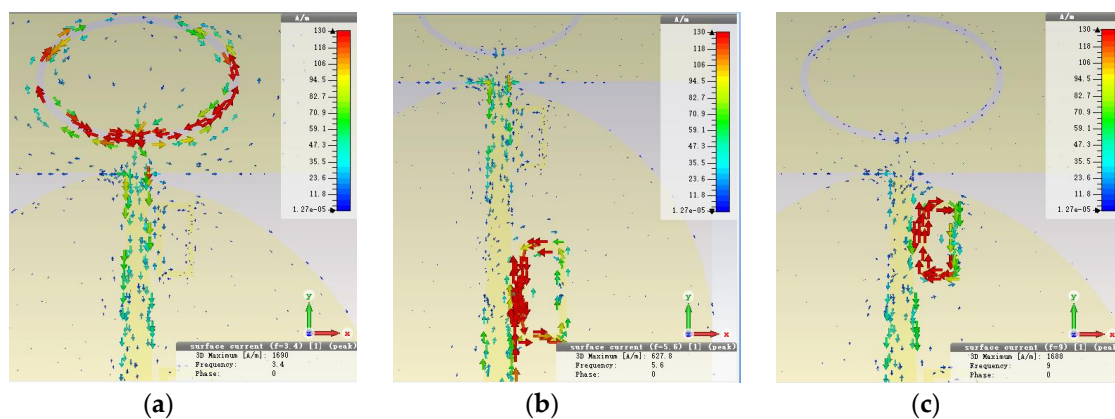
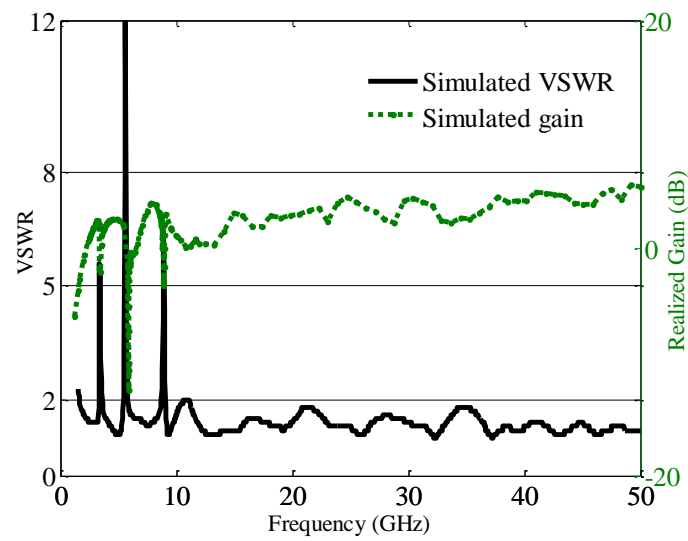
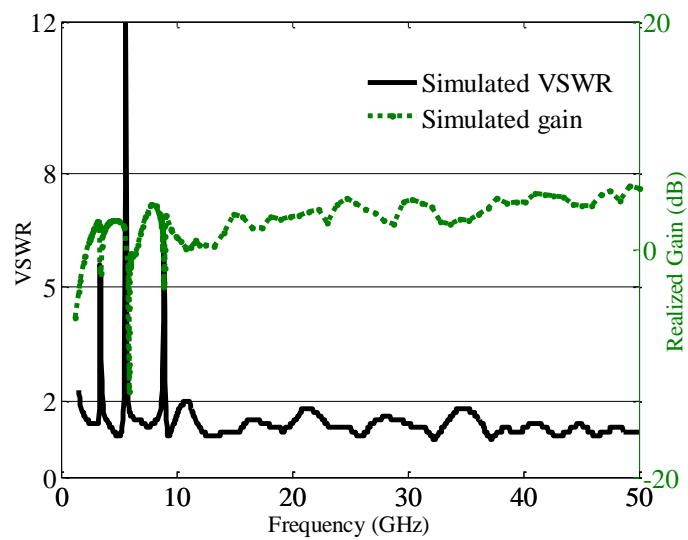


Figure 11. Current distribution at: (a) 3.4 GHz; (b) 5.6 GHz; (c) 9 GHz.

In order to measure the radiation pattern and gain of the antenna, the chamber was calibrated by placing a Standard Gain Horn (SGH) antenna at an antenna positioner. After calibration, the antenna was placed at the same location and, keeping all other RF configurations fixed, automated software calculated its accurate gain by dividing SGHs with the response of the actual antenna. The realized peak gain for the SWB antenna was about 3–5 dB. Figure 12a,b show the plot of simulated and measured VSWR versus gain for the SWB antenna. The gain was measured at selected frequencies from 2 GHz to 40 GHz. From measured and simulated results, it can be seen that there was a sharp decrease in the frequency band at 3.4, 5.6 and 9 GHz, while at other frequencies the antenna showed satisfactory performance. The co- and cross-polar patterns are shown in Figure 13a–d. It is observed that near omnidirectional, co-polar patterns were achieved in H-plane. In E-plane and H-plane, the cross-polarization was lower than co-polarization, however at some frequencies, the cross-polarization level rose due to the horizontal component of surface current on the radiation patch at some high frequencies.

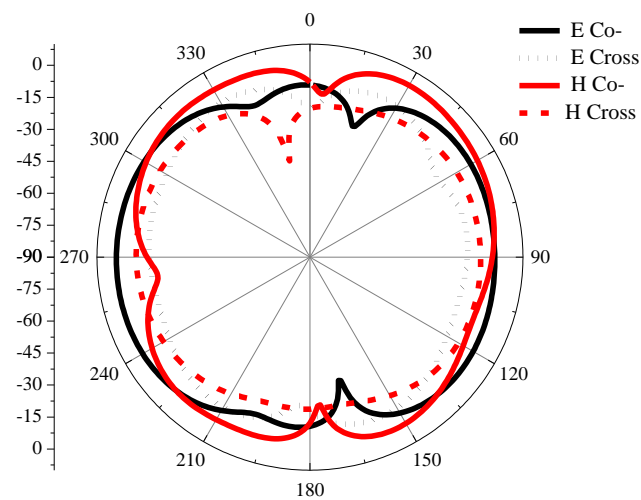


(a)



(b)

Figure 12. The plot of VSWR versus gain: (a) Simulated; (b) measured.



(a)

Figure 13. Cont.

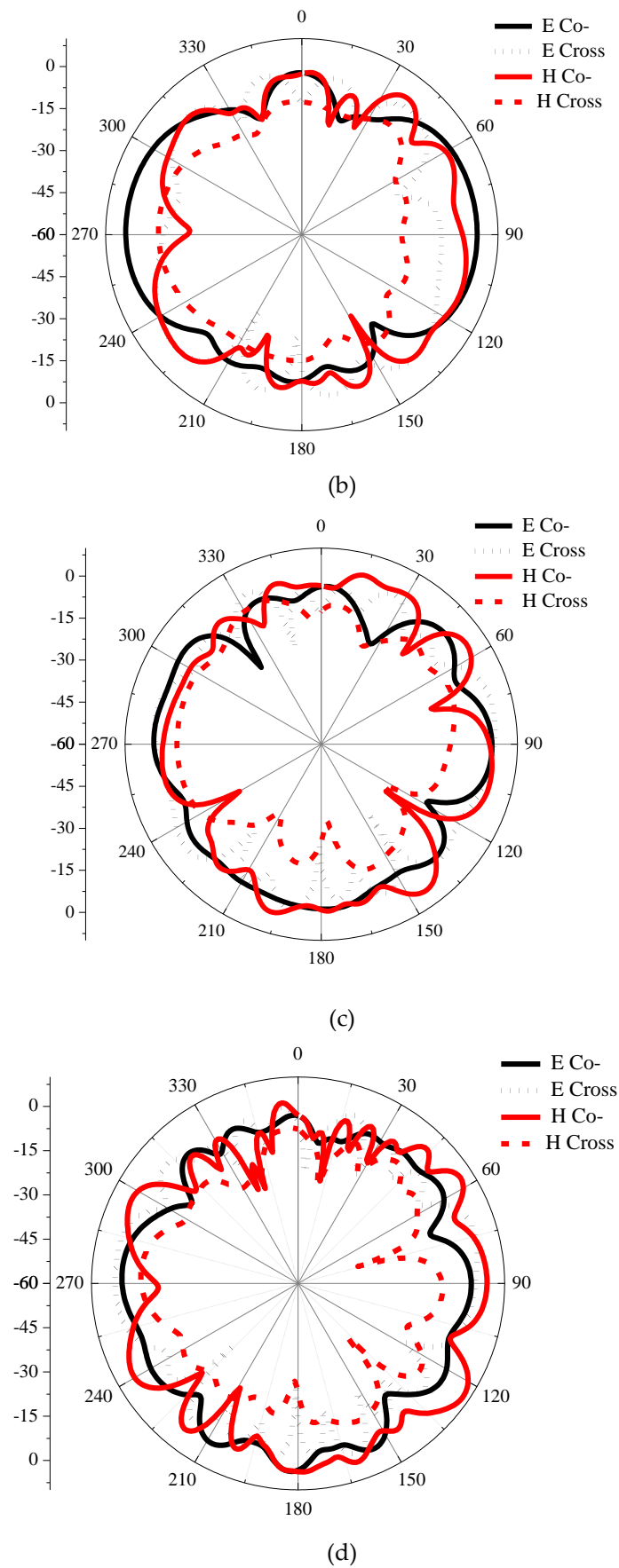


Figure 13. The co- and cross-polar pattern at: (a) 10 GHz; (b) 20 GHz; (c) 30 GHz; and (d) 40 GHz in both E- and H-plane.

The efficiency plot with and without notch bands have been depicted in Figure 14. The average efficiency in the passband was 95.75%, with a maximum efficiency of 99.30%. The efficiency of the band notch antenna sharply decreased in the respected narrow band.

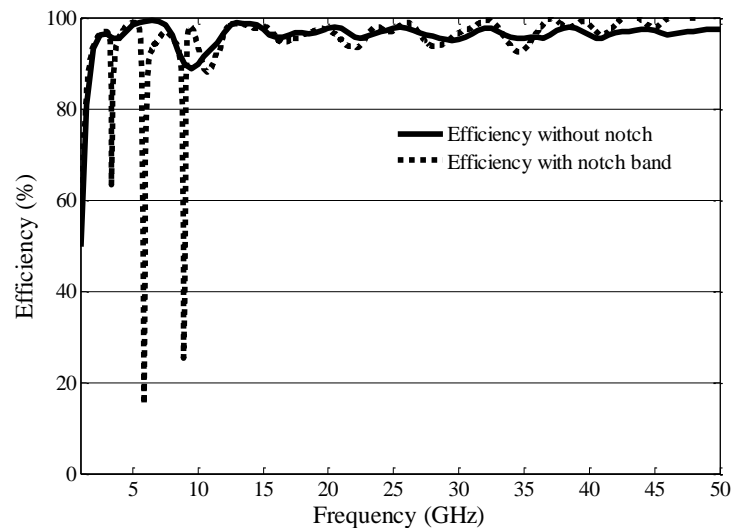


Figure 14. The plot of efficiency plot without and with notch bands.

4. Conclusions

In this paper, the SWB antenna has been designed and studied, which resonates from 1.42 GHz to 50 GHz. The interference of narrow bands was also reduced in the SWB range. The interference of narrow bands such as WLAN, WiMAX, and X band were suppressed by loading two RSRRs near the signal line and etching out the ESRR from the radiator. The antenna provided three stop band resonance frequencies at 3.4, 5.6 and 9 GHz. Moreover, a varactor diode was incorporated into the isolated area in ESRR, which can tune the first band from 1.9 GHz to 2.5 GHz by changing the capacitance of the varactor diode. Finally, the realized gain and current distribution of the notch characteristics antenna has shown the interference rejection at the desired stop band resonance frequencies. Due to these advantages, the designed antenna structure will be useful for ISM, Wi-Fi, WLAN, WiMAX, C, S, X, K, and Ku wireless communication systems.

Author Contributions: Writing: Original draft preparation was made by S.U.R., while reviewed by X.Z., I.G., M.I.K. and supervised by Q.C.

Funding: This research received no external funding.

Acknowledgments: The authors gratefully acknowledge the College of Electronic and Information Engineering, Nanjing University of Aeronautics and Astronautics (NUAA), Nanjing and Guangdong University of Technology, Guangzhou for providing the necessary facilities in particular Prof. Qunsheng Cao for supervising us. Mr. Saeed Ur Rahman acknowledge the Intelligent Computation and Application Research of Electromagnetics (ICARE) lab for its support.

Conflicts of Interest: The authors declare no conflict of interest.

References

1. Liu, J.; Esselle, K.P.; Member, S.; Hay, S.G.; Sun, Z. A Compact Super-Wideband Antenna Pair With Polarization Diversity. *IEEE Antennas Wirel. Propag. Lett.* **2013**, *12*, 1472–1475. [[CrossRef](#)]
2. Barbarino, S.; Consoli, F. Study on Super-Wideband Planar Asymmetrical Dipole Antennas of Circular Shape. *IEEE Trans. Antennas Propag.* **2010**, *58*, 4074–4078. [[CrossRef](#)]
3. Manohar, M.; Kshetrimayum, R.S.; Gogoi, A.K. Printed monopole antenna with tapered feed line, feed region and patch for super wideband applications. *IET Microw. Antennas Propag.* **2014**, *8*, 39–45. [[CrossRef](#)]

4. Singhal, S.L.; Singh, A.K. CPW-fed octagonal super-wideband fractal antenna with defected ground structure. *IET Microw. Antennas Propag.* **2017**, *11*, 370–377. [[CrossRef](#)]
5. Palaniswamy, S.K.; Kanagasabai, M.; Arun Kumar, S.; Alsath, M.G.N.; Velan, S.; Pakkathillam, J.K. Super wideband printed monopole antenna for ultra wideband applications. *Int. J. Microw. Wirel. Technol.* **2017**, *9*, 133–141. [[CrossRef](#)]
6. Liu, J.; Esselle, K.P.; Hay, S.G.; Zhong, S.S. Study of an Extremely Wideband Monopole Antenna With Triple Band-Notched Characteristics. *Prog. Electromagn. Res.* **2012**, *123*, 143–158. [[CrossRef](#)]
7. Yeo, J.; Lee, J.-I. Coupled-sectorial-loop antenna with circular sectors for superwide band application. *Microw. Opt. Technol. Lett.* **2014**, *56*, 1683–1689. [[CrossRef](#)]
8. Azari, A. A New Super Wideband Fractal Microstrip Antenna. *IEEE Trans. Antennas Propag.* **2011**, *59*, 1724–1727. [[CrossRef](#)]
9. Chen, K.R.; Sim, C.Y.D.; Row, J.S. A Compact Monopole Antenna for SuperWideband Applications. *IEEE Antennas Wirel. Propag. Lett.* **2011**, *10*, 488–491. [[CrossRef](#)]
10. Dong, Y.; Hong, W.; Liu, L.; Zhang, Y.; Kuai, Z. Performance analysis of a printed super-wideband antenna. *Microw. Opt. Technol. Lett.* **2009**, *51*, 949–956. [[CrossRef](#)]
11. Siddiqui, J.Y.; Saha, C.; Antar, Y.M.M. Compact SRR loaded UWB circular monopole antenna with frequency notch characteristics. *IEEE Trans. Antennas Propag.* **2014**, *62*, 4015–4020. [[CrossRef](#)]
12. Azim, R.; Mobashsher, A.T.; Islam, M.T. UWB antenna with notched band at 5.5 GHz. *Electron. Lett.* **2013**, *49*, 922–924. [[CrossRef](#)]
13. Azim, R.M.; Islam, T.; Mobashsher, A.T. Dual band-notch UWB antenna with single tri-arm resonator. *IEEE Antennas Wirel. Propag. Lett.* **2014**, *13*, 670–673. [[CrossRef](#)]
14. Zhang, C.; Zhang, J.; Li, L. Triple band-notched UWB antenna based on SIR-DGS and fork-shaped stubs. *Electron. Lett.* **2014**, *50*, 67–69. [[CrossRef](#)]
15. Wang, J.; Wang, Z.; Yin, Y.; Liu, X. UWB Monopole Antenna with Triple Band-Notched Characteristic Based on a Pair of Novel Resonators. *Prog. Electromagn. Res. C* **2014**, *49*, 1–10. [[CrossRef](#)]
16. Cai, Y.-Z.; Yang, H.-C.; Cai, L.-Y. Wideband Monopole Antenna With Three Band-Notched Characteristics. *IEEE Antennas Wirel. Propag. Lett.* **2014**, *13*, 607–610.
17. Rahman, S.U.; Cao, Q.; Wang, Y.; Ullah, H. Design of wideband antenna with band notch characteristics based on single notching element. *Int. J. RF Microw. Comput. Aided Eng.* **2019**, *29*, e21541. [[CrossRef](#)]
18. Rahman, S.U.; Cao, Q.; Li, Y.; Gil, I.; Yi, W. Design of tri-notched UWB antenna based on elliptical and circular ring resonators. *Int. J. RF Microw. Comput. Aided Eng.* **2019**, *29*, e21648. [[CrossRef](#)]
19. Rahman, M.; Dong, K.; Jung, D.P. A Compact Multiple Notched Ultra-Wide Band Antenna with an Analysis of the CSRR-TO-CSRR Coupling for Portable UWB Applications. *Sensors* **2017**, *17*, 2174. [[CrossRef](#)]
20. Almalkawi, M.J.; Devabhaktuni, V.K. Quad band-notched UWB antenna compatible with WiMAX/INSAT/lower-upper WLAN applications. *Electron. Lett.* **2011**, *47*, 1062–1063. [[CrossRef](#)]
21. Rahman, M.; Park, J.D. The Smallest Form Factor UWB Antenna with Quintuple Rejection Bands for IoT Applications. *Sensors* **2018**, *18*, 911. [[CrossRef](#)] [[PubMed](#)]
22. Mewaraa, H.S.; Jitendra, K.D.; Mahendra, M.S. A slot resonators based quintuple band-notched Y-shaped planar monopole ultra-wideband antenna. *Int. J. Electron. Commun.* **2018**, *83*, 470–478. [[CrossRef](#)]
23. Shahsavari, H.; Nourinia, J.; Shirzad, H.; Shokri, M.; Asiaban, S.; Amiri, Zh.; Virdee, B. Compact planar super-wideband antenna with band-notched function. *Appl. Comput. Electromagn. Soc. J.* **2013**, *28*, 608–613.
24. Manohar, M.; Kshetrimayum, R.S.; Gogoi, A.K. Super wideband antenna with single band suppression. *Int. J. Microw. Wirel. Technol.* **2017**, *9*, 143–150. [[CrossRef](#)]
25. Abbas, A.S.; Abdelazeez, M.K. A dual band notch planar SWB antenna with two vertical sleeves on slotted ground plane. In Proceedings of the IEEE International Symposium on Antennas and Propagation (APSURSI), Fajardo, Puerto Rico, 26 June–1 July 2016.
26. Manohar, M.; Kshetrimayum, R.S.; Gogoi, A.K. A compact dual band-notched circular ring printed monopole antenna for super-wideband applications. *Radioengineering* **2017**, *26*, 64–70. [[CrossRef](#)]
27. Ghafouri-Shiraz, H.; Rabbani, M.S. Simple methods for enhancing bandwidth of a rectangular microstrip patch antenna. In Proceedings of the 2nd IET Annual Active and Passive RF Devices Seminar, Birmingham, UK, 29 October 2014; pp. 1–4.
28. Balanis, C.A. *Antenna Theory: Analysis and Design*, 3rd ed.; Hoboken, NJ, USA: John Wiley, 2005.

29. Tang, M.; Ziolkowski, R.W.; Xiao, S. Compact Hyper-Band Printed Slot Antenna With Stable Radiation Properties. *IEEE Trans. Antennas Propag.* **2014**, *62*, 2962–2969. [[CrossRef](#)]
30. Abhik, G.; Anirban, K.; Manimala, P.; Rowdra, G. A Cpw-Fed Propeller Shaped Monopole Antenna With Super Wideband Characteristics. *Prog. Electromagn. Res. C* **2013**, *45*, 125–135.
31. Hakimi, S.; Rahim, K.A.; Abedian, M.; Noghabaei, S.M.; Khalily, M. CPW-Fed transparent antenna for extended ultrawideband applications. *IEEE Antennas Wirel. Propag. Lett.* **2014**, *13*, 1251–1254. [[CrossRef](#)]
32. Mohammad, R.A.; Dorostkar, A.; Mohammad, T.I. Design of a novel super wide band circular-hexagonal fractal antenna. *Prog. Electromagn. Res.* **2013**, *139*, 229–245.
33. Rahman, M.N.; Islam, M.T.; Mahmud, M.Z.; Samsuzzaman, M. Compact microstrip patch antenna proclaiming super wideband characteristics. *Microw. Opt. Technol. Lett.* **2017**, *59*, 2563–2570. [[CrossRef](#)]
34. Singhal, S.; Singh, A.K. CPW-fed hexagonal Sierpinski super wideband fractal antenna. *IET Microw. Antennas Propag.* **2016**, *10*, 1–7. [[CrossRef](#)]
35. Zhong, S.S.; Liu, J.; Hay, S.G.; Esselle, K.P. Compact super-wideband asymmetric monopole antenna with dual-branch feed for bandwidth enhancement. *Electron. Lett.* **2013**, *49*, 515–516.
36. Srifi, M.N.; Mrabet, O.; Falcone, F.; Ayza, M.S.; Essaaidi, M.; Ghz, F. A Novel Compact Printed Circular Antenna For Very Ultrawideband Applications. *Microw. Opt. Technol. Lett.* **2009**, *51*, 1130–1133. [[CrossRef](#)]
37. Shahu, B.L.; Pal, S.; Chattoraj, N. Design of Super Wideband Hexagonal-Shaped Fractal Antenna with Triangular Slot. *Microw. Opt. Technol. Lett.* **2015**, *57*, 1659–1662.
38. Srifi, M.N.; Podilchak, S.K.; Essaaidi, M.; Antar, Y.M.M. Compact disc monopole antennas for current and future ultrawideband (UWB) applications. *IEEE Trans. Antennas Propag.* **2011**, *59*, 4470–4480. [[CrossRef](#)]
39. Sarkar, D.; Srivastava, K.V.; Saurav, K. A compact microstrip-fed triple band-notched UWB monopole antenna. *IEEE Antennas Wirel. Propag. Lett.* **2014**, *13*, 396–399. [[CrossRef](#)]



© 2019 by the authors. Licensee MDPI, Basel, Switzerland. This article is an open access article distributed under the terms and conditions of the Creative Commons Attribution (CC BY) license (<http://creativecommons.org/licenses/by/4.0/>).